applied nano

MDPI

Article

A Methodology for Validation of DNA Origami–Quantum Dot Hybridization

Mathis Janßen [1,*], Anastasiia D. Murkina [2], Julia Hann [1], Gunnar Klös [2], Martin Moebius [1], Christoph R. Meinecke [1,3], Andreas Morschhauser [1,3], Aitziber L. Cortajarena [2,4] and Danny Reuter [1,3]

1 Center for Micro and Nano Technologies, University of Technology Chemnitz, Reichenhainer Str. 70, 09126 Chemnitz, Germany; julia.hann@zfm.tu-chemnitz.de (J.H.); christoph.robert.meinecke@enas.fraunhofer.de (C.R.M.)
2 Center for Cooperative Research in Biomaterials (CIC biomaGUNE), Basque Research and Technology Alliance (BRTA), Paseo de Miramón 194, 20014 Donostia-San Sebastián, Spain; amurkina@cicbiomagune.es (A.D.M.); gklos@cicbiomagune.es (G.K.); alcortajarena@cicbiomagune.es (A.L.C.)
3 Fraunhofer Institute for Electronic Nanosystems (ENAS), Technologie-Campus 3, 09126 Chemnitz, Germany
4 IKERBASQUE, Basque Foundation for Science, Plaza Euskadi 5, 48009 Bilbao, Spain
* Correspondence: mathis.janssen@zfm.tu-chemnitz.de

Abstract

Since the introduction of the DNA origami technology by Seeman and Rothemund, the integration of functional entities (nanoparticles, quantum dots, antibodies, etc.) has been of huge interest to broaden the area of applications for this technology. The possibility of precise functionalization of the DNA origami technology gives opportunity to build up complex novel structures, opening up endless opportunities in medicine, nanotechnology, photonics and many more. The main advantage of the DNA origami technology, namely the self-assembly mechanism, can represent a challenge in the construction of complex mixed-material structures. Commonly, DNA origami structures are purified post-assembly by filtration (either spin columns or membranes) to wash away excess staple strands. However, this purification step can be critical since these functionalized DNA origami structures tend to agglomerate during purification. Therefore, custom production and purification procedures need to be applied to produce purified functionalized DNA origami structures. In this paper, we present a workflow to produce functionalized DNA origami structures, as well as a method to qualify the successful hybridization of a quantum dot to a square frame DNA origami structure. Through the utilization of a FRET fluorophore–quencher pair as well as a subsequent assembly, successful hybridization can be performed and confirmed using photoluminescence measurements.

Keywords: DNA origami; self-assembly; functionalization; quantum dots; hybridization; nanotechnology; Foerster-resonance electron transfer quenching; fluorophore; quencher

check for updates

Academic Editors: Paolo Mele, Cristiano Giordani and Marco Fronzi

Received: 3 November 2025
Revised: 24 November 2025
Accepted: 1 December 2025
Published: 8 December 2025

Citation: Janßen, M.; Murkina, A.D.; Hann, J.; Klös, G.; Moebius, M.; Meinecke, C.R.; Morschhauser, A.; Cortajarena, A.L.; Reuter, D. A Methodology for Validation of DNA Origami–Quantum Dot Hybridization. *Appl. Nano* **2025**, *6*, 30. https://doi.org/10.3390/applnano6040030

Copyright: © 2025 by the authors. Licensee MDPI, Basel, Switzerland. This article is an open access article distributed under the terms and conditions of the Creative Commons Attribution (CC BY) license (https://creativecommons.org/licenses/by/4.0/).

1. Introduction

Over the past 15 years, DNA origami (DO) has emerged as a powerful tool for the bottom-up assembly of nanostructures, with unprecedented spatial control at the nanometer scale [1–3]. The ability to precisely fold a long scaffold strand into predefined two- and three-dimensional shapes, through the hybridization of short staple strands, has enabled the development of complex architectures for applications in medicine, nanotechnology, photonics, etc. [4]. One of the most compelling advantages of DO is its capability to serve as a programmable platform for the integration of functional entities, such as nanoparticles,

quantum dots (QDs), and antibodies, which significantly expand its potential applications [4].

In particular, QDs with sizes around 10 nm are suitable for integration into DO [5]. In these semiconductor nanoparticles, the charge carriers are strongly confined in all three dimensions, which leads to the emergence of discrete energy levels and size-dependent photophysical behavior. The resulting process of photoluminescence (PL) finds broad application in many fields [6,7]. Thereby, the wavelength of the emitted photons and electronic properties can be tuned by adjusting their size and surface chemistry during synthesis [8].

However, DO provides unmatched spatial addressability (~2–5 nm) [9]. When functional elements are introduced, issues such as aggregation, non-specific binding, and loss of structural integrity during purification can arise [10].

Due to their nanometer-scale size, the structural characterization of DO structures is limited to high-resolution imaging techniques. Atomic force microscopy is the most commonly used method for directly visualizing the topography and structural integrity of DO. However, the time-consuming nature of this method, coupled with limitations in the size of the examination area and its dependence on surface fixation, has led to the development of alternative fluorescence-based imaging techniques, such as stochastic optical reconstruction microscopy (STORM) and DNA points accumulation for imaging in nanoscale topography (DNA-PAINT) [11]. The latter uses transient hybridization of short, dye-labeled DNA imager strands and staple overhangs on the surface of the DO, while STORM uses the stochastic switching on and off of individual fluorophores for precise localization of individual molecules. While these methods can map the position of the staple overhangs integrated into the origami, they do not allow validation of the actual integration of the functional element. These limitations highlight the need for new fluorescence-based approaches that enable the sensitive and specific characterization of functional elements attached to DO structures.

Standard purification methods, including spin-column filtration and membrane-based separation, are often associated with significant material loss or undesired agglomeration of the modified functionalized structures for functionalized DO [10]. Thus, there is a growing need for optimized workflows that ensure the stable incorporation and purification of functionalized DNA origami structures without compromising their integrity.

Photoluminescence (PL) is a widely used optical technique for characterizing the interaction between fluorophores, quenchers, and nanomaterials in functionalized DNA origami structures [12]. When a material absorbs photons, it transitions to an excited electronic state and subsequently relaxes by emitting light [9]. This property is particularly useful in DNA origami studies where the Förster Resonance Energy Transfer (FRET) mechanism can be applied to monitor hybridization events and interactions at the nanoscale [13].

In the context of this study, PL measurements serve as a crucial tool for validating the successful conjugation of quantum dots to DNA origami structures. By analyzing the PL emission spectra, we can confirm the presence of quantum dots on the DNA scaffold and assess the structural integrity of the functionalized assembly. This approach ensures a reliable method for evaluating DNA origami-based nanostructures, with potential applications in biosensing, imaging, and nanophotonics.

Importantly, beyond providing a verification tool, the methodology developed here demonstrates that DNA origami can reliably template individual QDs with nanometer precision, enabling highly controlled architectures that are otherwise difficult to achieve. Such deterministic positioning of single QDs is a key step toward programmable nanophotonic device fabrication, which illustrates the broader technological relevance of the assembly strategies presented in this work [14].

2. Materials and Methods

2.1. DNA Origami Design and Simulation

The structure was designed using CaDNAno v2.0 software [15]. It features a two-layer, 2D square lattice with dimensions of 61.2 × 72 × 2 nm^3 and a central gap measuring 30 × 28 nm^2. Four single-stranded overhangs extend from the edges of this gap, enabling hybridization with a QD. Additionally, two single-stranded sequences protrude from the outer edges, facilitating controlled surface attachment or further polymerization. Structural simulations were conducted using CanDo [16], which employs finite element analysis. In this process, all double helices are arranged linearly, with strand crossovers treated as rigid constraints. External forces (stretching, bending, and torsional forces) are then applied to deform the structure, positioning crossovers between the involved helices. When the structure exhibits internal strain during the nonlinear finite element analysis, incompatibility with B-form DNA geometry is assumed [16,17].

2.2. DNA Origami Assembly and Purification

As initial step for the assembly process, all staple sequences (Invitrogen by Thermo Fisher Scientific, Carlsbad, CA, USA) were combined and diluted to a concentration of 0.2 µM. The assembly buffer (10 mM Tris, 10 mM $MgCl_2$, and 1 mM EDTA in filtered, deionized water) was autoclaved and subsequently used for the preparation of multiple 50 µL assembly batches, each containing 10 µL of the staple pool, 5 µL of the scaffold, and 35 µL of assembly buffer. Self-assembly was carried out in a thermocycler (Prime technologies), with the temperature gradually decreasing from 85 °C to 25 °C at a rate of −1 K/min. After assembly, all batches were combined and purified using 10 mM Tris with 10 mM $MgCl_2$ as the purification buffer, along with 0.5 mL Amicon centrifuge filters (Merck, Darmstadt DEU). The concentration of the purified DNA structures was then measured using UV/Vis spectrometry (Uviline 9400, Schott, Mainz DEU). To this end, the purification buffer was utilized as a blank.

2.3. Quantum Dot Synthesis and Biofunctionalization

Chemicals. L-Glutathione (GSH, reduced, 98+%, Thermo Fisher Scientific, Waltham, MA, USA), ammonium citrate dibasic (ACS reagent grade, 98%, Sigma–Aldrich, St. Louis, MO, USA), ammonia solution (NH_4OH, 28–30%, Sigma–Aldrich), indium(III) chloride ($InCl_3$, 99.999%, Sigma–Aldrich), silver nitrate ($AgNO_3$, ACS reagent, ≥99.0%, Sigma–Aldrich), sodium sulfide nonahydrate ($Na_2S{\cdot}9H_2O$, ≥98.0%, Sigma–Aldrich), and zinc acetate dihydrate ($Zn(CH_3COO)_2 \times 2H_2O$, ACS reagent, ≥98%, Sigma–Aldrich) were used. All the chemicals were used without further purification.

DNA sequences. DNA oligonucleotides were purchased from biomers.net GmbH.
Pair 1: 5′-ACGTCGTAGTACCCTGATGCATGTAAAAAAAAAA[Thiol]-3′;
5′-[Thiol]AAAAAAAAAAATGTCGTACGTTCGAGATCGATCG-3′.
Pair 2: 5′-ACGTCGTAGTACCCTGATGCATGT[BHQ2]-AAAAAAAAAA[Thiol]-3′;
5′-[Thiol]AAAAAAAAAA-AT[BHQ2]GTCGTACGTTCGAGATCGATCG-3′.

$AgInS_2$ (AIS) QDs with an emission wavelength of 635 nm and a quantum yield of 80% were utilized for the work presented here. For the core QDs, 8 mL of 0.1 M aqueous GSH and 70 mg of ammonium citrate were introduced into a three-neck flask. The pH was adjusted to 6.5 with NH_4OH (5 M). Then, 0.5 mL of 1 M aqueous $InCl_3$ was added, resulting in the development of a precipitate. Subsequently, NH_4OH was introduced until the precipitate was fully dissolved, and the mixture's pH returned to 6.5. The mixture was heated to 96 °C. A rapid injection of 250 µL of 0.1 M aqueous $AgNO_3$ and 125 µL of 1 M aqueous Na_2S was performed to create the AIS seeds. Subsequently, 1 mL of 0.1 M aqueous $AgNO_3$ and 500 µL of 1 M aqueous Na_2S were slowly and successively added drop by

drop. The mixture was maintained at 96 ° C while being stirred for 1 h. Fluorescence emission spectra for AIS-QDs were acquired using an FS5 spectrofluorometer, (Edinburgh Instruments, Livingston GBR) with an excitation wavelength of 465 nm, a slit width of 1 nm, a 1 nm data interval, and an averaging time of 0.2 s.

The design of the hybridization sequences for Pair 1 and Pair 2 specifically aimed to avoid significant alignment with other staple sequences. Sequence analysis revealed only short partial matches of up to 7 bases with 2 staples, confirming that the hybridization sequences are appropriate for the intended specific hybridization. DNA oligonucleotides meant for hybridization with the DO were linked to the ZnS shell during its synthesis. To this end, 100 µL of the core QDs solution was diluted in 5 mL of Milli-Q water and heated to 96 °C. Subsequently, 2 mL of an aqueous solution containing 97 µL of $Zn(CH_3COO)_2 \times 2H_2O$ stock solution (0.1 M) and two sequences of thiolated single-stranded DNA (with a ssQDs/DNA concentration ratio of 1/10) was added, along with 2 mL of another aqueous solution containing 9.7 µL Na_2S (1 M), which was added dropwise and simultaneously. In the case of the QD biofunctionalization with BHQ2 (2. sequence pair, see DNA sequences section), the precursors for the QD shell were added first, followed by the addition of DNA with BHQ2. This order of addition was essential, as injection of BHQ2 and shell precursors simultaneously led to coagulation of the QDs. Following the addition, the mixture was incubated at 96 °C for 1 h. Ultimately, functionalized QDs were purified by centrifugation using an Amicon centrifugal filter [18].

2.4. Hybridization with Functionalized Quantum Dots

The hybridization of the DNA origami with the functionalized QD was performed by annealing of 10 µL of 10 nM of purified DO structures with 2 µL of 0.5 µM functionalized QDs for 60 min in a thermocycler (Techne by Cole-Parmer, Vernon Hills, IL, USA). The thermocycler program consists of 20 min of storage at 50 °C and subsequent cooling to 10 °C at a rate of −1K/min. All structures were stored at 4 °C after purification until further utilization.

2.5. Purification and Qualification of Functionalized Structures

Hybrid structures were purified by gel electrophoresis. To this end, 1% agarose gels were cast (10 mM Tris supplemented with 10 mM $MgCl_2$ as gel-casting and running buffer) and prestained with GelRed intercalating dye (Sigma–Aldrich/Merck). The gels were run at 90 V for 90 min. Gel documentation was performed with a DarkHood DH-50 (BioStep, Burkhardtsdorf DEU) alongside the argus x1 documentation software (BioStep). Bands correlating to hybrid structures were cut out and placed into filtered pipette tips fitted into 1.5 mL tubes and stored at −22 °C over night. Next, these spin filters were centrifuged for 5 min in a table centrifuge to recover the hybrid structures. Afterwards, the purified DO QD hybrids could be collected from the bottom of the tube.

2.6. Validation via Photoluminescence Measurements

In order to validate the successful hybridization of only a single quantum dot to a single DO structure, different variations in DO, QDs, and hybrids were investigated via photoluminescence measurements. The samples were excited using a confocal setup consisting of a microscope and camera (AXIO Imager Z2m, Axiocam 305, Carl Zeiss AF, Oberkochen DEU) with a coupled laser operating at a wavelength of 475 nm. The resulting photoluminescence (PL) was then directed to the spectrometer system (Andor Shamrock SR-303i-A and Newton DU920P-BEX2-DD, Belfast GBR) via optical fiber for spectral analysis. Table 1 gives an overview of all samples measured. All hybrids (DO + QD) presented in the table were measured as crude samples as well as purified ones. A volume of 5 µL from each sample was deposited on a fresh glass slide and left to dry on air prior to the measurement.

As a reference, a cleaned glass slide was also measured. The glass slide was cleaned by subsequent ultra-sonic bath cleaning for 10 s in isopropanol, ethanol, and deionized water.

Table 1. Overview of samples investigated. Samples C–F were validated in crude as well as pure composition. All DNA origami solutions were prepared at 10 nM. In the following, samples will be abbreviated as follows: no fluorophore = −T, with fluorophore = +T, no quencher = −Q, and with quencher = +Q.

Sample	Description	Abbreviations
A	DNA Origami (no fluorophore)	DO (−T)
B	DNA Origami (with fluorophore)	DO (+T)
C	DNA Origami (no fluorophore) + QDs (no quencher)	DO (−T) + QDs (−Q)
D	DNA Origami (with fluorophore) + QDs (no quencher)	DO (+T) + QDs (+Q)
E	DNA Origami (no fluorophore) + QDs (with quencher)	DO (−T) + QDs (+Q)
F	DNA Origami (with fluorophore) + QDs (with quencher)	DO (+T) + QDs (+Q)

2.7. AFM Measurement and Gwyddion Data Processing

Mica immobilization was used to assess the structural integrity of individual DNA origami structures. Structures immobilized on mica were investigated with atomic force microscopy (AFM, FlexAFM, Nanosurf, Liestal CHE). For every immobilization, 5 µL of DO sample was immobilized on freshly cleaved mica plates. These samples were then incubated for 5 min and then rinsed with 150 µL of filtered deionized water. Afterwards, mica plates were dried with N_2 prior to measurement. For each immobilization, a 10 × 10 µm^2 overview and a 2 × 2 µm^2 detail image were recorded with 512 points/line and 0.98 s/line. All measurements were performed with PPP-NCHR tips (Nanosensors, Neuchatel CHE), with a vibrational frequency in the range of 301.869–330.714 kHz. The analysis of the image data was performed with the open-source software Gwyddion version 2.67 [19].

3. Results

The requirements arising from the subsequent use of the DNA origami structure for the separation and controlled surface integration of a QD were addressed by a specific frame design, shown in Figure 1. It shows the frame structure as CaDNAno design file (I) and as RMSF visualization of the simulated design (II).

The structure was designed with regard to rigidity. To this end, it was designed as a two-layer planar structure with plenty of internal layer crossovers (see Figure 1I,III). As is evident from Figure 1II, the structure features eight single-stranded overhangs extruding from the edges of the structure (for specialized surface immobilization, not relevant for this publication), as well as four single-stranded overhangs extruding from the inner corners of the structure. These inner overhangs were designed to feature a 23-base long sequence for the annealing of a complementary sequence and thus facilitate the hybridization to a single QD. Two different sequences were designed so that overhangs diagonally of each other have the same sequence (see Table 2). The corresponding $AgInS_2$ QDs were synthesized, resulting in photoluminescent QDs with an emission maximum at 650 nm (Figure 2). $AgInS_2$ QDs were functionalized with thiolated DNA strands containing the sequence required for hybridization with the DO, as well as an additional 10 A-segment linker with a terminal thiol group for QD functionalization. Thiol functionalization was used to orient the DNA sequence towards the quantum dot surface, after which the DNA is integrated into the QD during the shell growth procedure (see Figure 2). As is evident from Figure 2, the shell growth process (see Methods D) facilitated a shift in the PL peak towards smaller wavelengths (650 nm → ~630 nm), resulting in an emission at 630 nm for the fully functionalized QDs. For validation, the QD sequences were modified with an internal quencher (BHQ2), while the DO sequences were modified with a terminal corresponding

fluorophore. Upon successful hybridization, spatial proximity between the fluorophore and quencher leads to efficient quenching of the previously emitted fluorescence signal of the DO sequence.

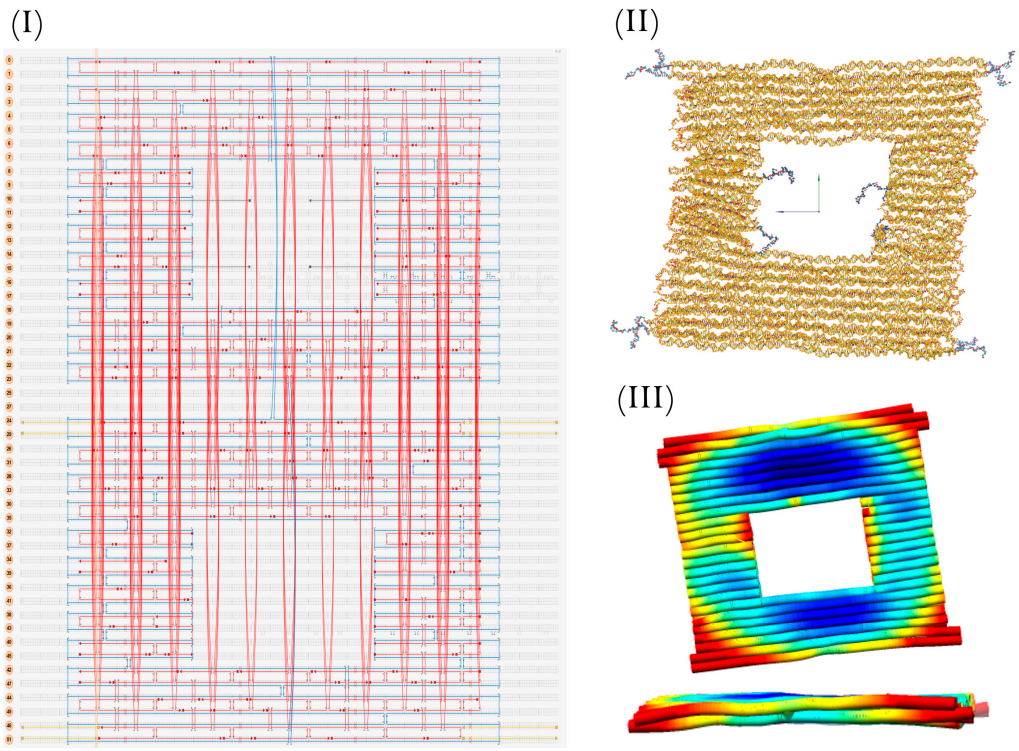


Figure 1. Various visualization of the frame structure: (**I**) CaDNAno schematic (scaffold = blue, staples = red, yellow & grey); (**II**) RMSF finite element simulation of the CaDNAno design via all-atom simulation via oxDNA; and (**III**) CanDo (bottom). oxView all-atom visualization of the frame structure was performed with the oxDNA online service [20].

Table 2. Overview of hybridization sequences; [-] marks the point in the sequence where it leaves or enters the DO structure; [Thiol] marks the functionalization of the DNA sequences with a thiol group. All sequences were produced with and without the fluorophore/quencher modification; however, duplicate sequence entries are not listed in the table. Reference [TAMRA] marks the integration of the fluorophore, while [BHQ2] marks the integration of the quenchers."QD_" labelled sequences attach to the QD, while all other sequences are integrated in the DO structure.

Name	**Sequence (5′ → 3′)**
TopLeft_F	[TAMRA]CATGCATCAGGGTACTACGACGT[-]TGGGCGCATCAAACCC
TopRight_F	AAAGACAAAAGGG[-]CGATCGATCTCGAACGTACGACA[TAMRA]
BottomRight_F	[TAMRA]CATGCATCAGGGTACTACGACGT[-]TTACCATTAGCAA
BottomLeft_F	TTTAACCAATAG[-]CGATCTGCTCGAACGTACGACA[TAMRA]
QD_TopLeft/BottomRight	ACGTCGTAGTACCCTGATGCATGT[BHQ2]AAAAAAAAAA[Thiol]
QD_TopRight/BottomLeft	[Thiol]AAAAAAAAAAAT[BHQ2]GTCGTACGTTCGAGATCGATCG

The specific quencher fluorophore combination was chosen due to the proximity of the respective peaks (TAMRA Emission = 583 nm, BHQ2 excitation = 579 nm).

Table 2 gives an overview of all sequences utilized for the hybridization of the DO with the QD, while Figure 3 visualizes the annealing of QD and DO exemplary for one sequence.

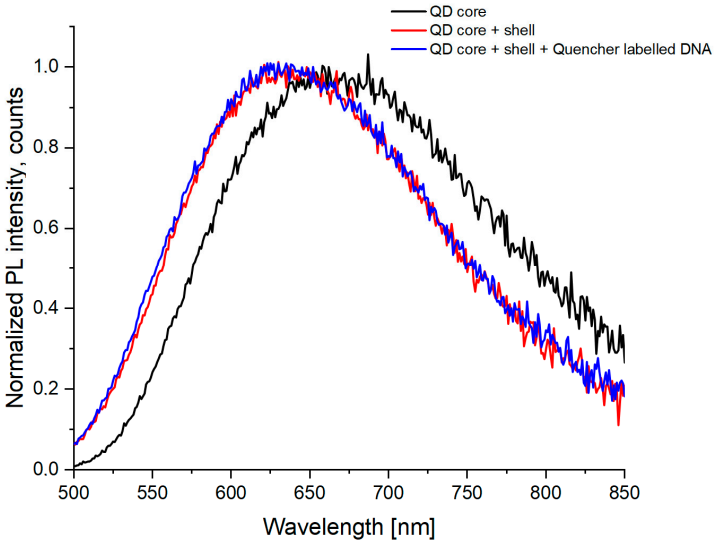


Figure 2. Photoluminescence emission spectra of AIS QDs (black), AIS QD with ZnS shell (red), and with quencher BHQ2 (blue) upon excitation at 465 nm.

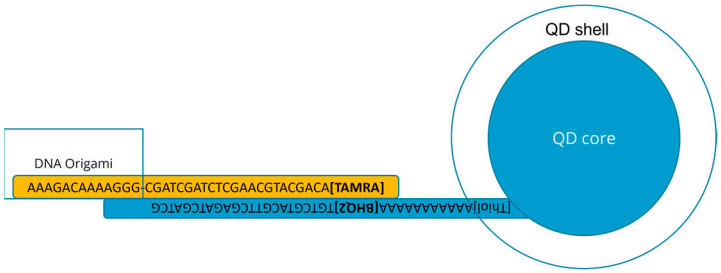


Figure 3. Visualization of validation principle: The DO-sequences features a terminal TAMRA-label resulting in a fluorescence signal for DO structures without QDs. During the annealing process, the fluorophore base modification (yellow strand extruding from the DNA origami) undergoes quenching by the Black Hole 2 Quencher (BHQ2), which is incorporated as a base modification in the DNA sequence that extrudes from the QD. Subsequent to successful annealing, the molecular weight of the product hybrid structure is increased (compared to the educts) and thus runs slower during gel electrophoresis.

The self-assembly of the frame structure was performed with two sets of staple pools, one of which featured TAMRA-labeled QD-hybridization sequences and one set that did not feature any fluorophore labeling. Samples A (without fluorophore) and B (with fluorophore) were produced, and subsequently a 10 µL of 10 nM purified frame structure solution (per sample) was used for the production of samples C-F. The full volume (~10 µL) of each sample was utilized for gel electrophoresis in order to minimize sample dilution.

Figure 4 shows the bands documented for all samples after gel electrophoresis. For samples B, D, and F, very intense bands are visible, while other bands appear rather weak. This is due to the emission of the fluorophore incorporated into these samples (see Table 1). All sample bands appear to have run slightly less far in the gel than the scaffold control sample. There is evidence for successful self-assembly of the structures since folded structures, due to their increased molecular weight, tend to migrate more slowly compared to the M13mp18 scaffold [15]. Gel extraction (see Methods E.) yielded about 50 µL per sample, resulting in an estimated concentration of 2 nM QD-DO hybrid structures.

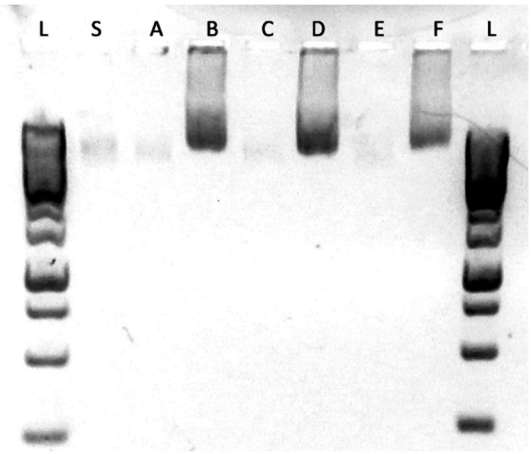


Figure 4. Image of 1% agarose gel after running for 90 min after 90 V. GelRed was used as gel stain. L = Ladder 1 kB, S = scaffold p7249, and samples A–F correspond to Table 1.

Figure 5 shows the results for the photoluminescence measurements of the samples. In Figure 5I, the photoluminescence of the DNA origami (without QD) with and without the TAMRA-fluorophore was measured. For both samples, a small peak at ~700 nm was detected, which corresponds to the glass slide. In Figure 5V, the yellow graph represents the PL measurements for a blank glass slide. Due to the confocal measurement setup, no exact measurement of total light intensity was possible, resulting in differences for sample A and the blank glass slide. Based on that result, it was assumed that DNA origami structures exhibit no photoluminescence for the investigated wavelength range (500–800 nm). sample B (red in Figure 5I)) shows a sharp peak at 583 nm. This peak corresponds to the TAMRA-fluorophore, which was incorporated into samples B, D, and F. In Figure 5II, samples C and D show similar graphs but with different peak intensities.

While the peak position (~625–650 nm) corresponds to the QDs, for sample D, the peak intensity is higher and tailing (see red graph in Figure 5II) can be observed. This is most likely due to the integrated fluorophore in sample D and the proximity of the fluorophore peak (583 nm) to the QD peak (~625–650 nm). Figure 5III shows the comparison in total photoluminescence counts for samples E and F. Sample F shows a higher peak intensity, which could indicate quenching of the QDs by the quencher. This assumption is supported by the normalized measurements of the samples C, E, and F in Figure 5IV. The graphs overlap, which suggests that the fluorophore is successfully quenched. Differences in total measured intensities were expected due to variations in DO density on the glass slide. Figure 5V shows the measurement of total photoluminescence counts for all samples, including the blank glass slide.

In parallel to photoluminescence investigations, AFM imaging of purified QD-DO hybrids as well as unfunctionalized DO structures immobilized on freshly cleaved mica was performed [21]. Figure 6 shows AFM images (I and II), as well as extracted height profiles (III and IV) for both DO-QD hybrids and DO structures [19]. They show a structure height of 2 to 3 nm for the DO template with a significant groove in the center of the structure for the functionalization with the QDs (see Figure 6I). After hybridization, this groove is no longer visible in either the topography image or the height profile due to the binding of the QD (see Figure 6II,IV).

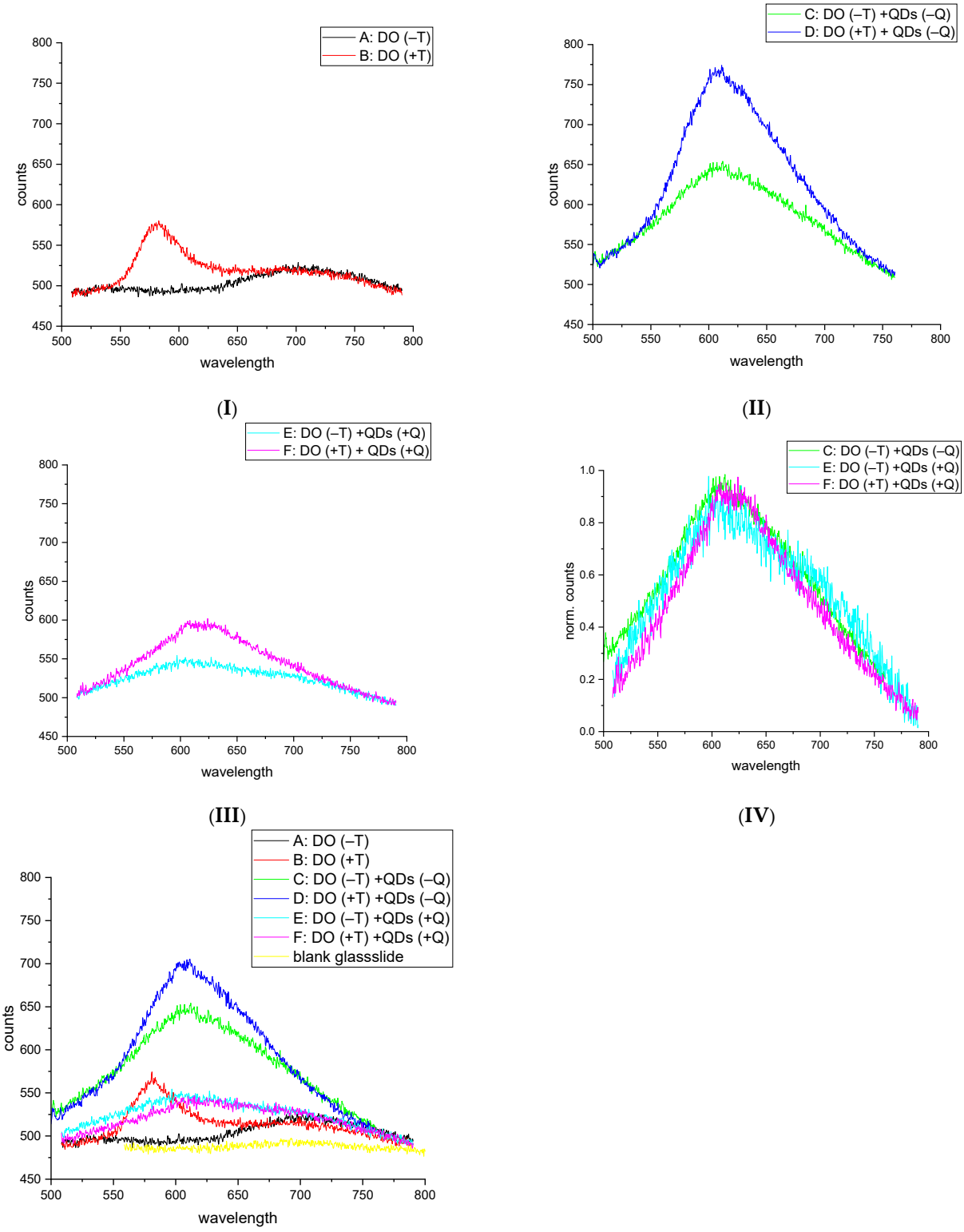


Figure 5. Photoluminescence measurements: (**I**) DNA origami with (sample B) and without (sample A) TAMRA-fluorophore and without QDs (total counts); (**II**) DNA origami with (sample D) and without (sample C) TAMRA-fluorophore and with QDs (without quencher) (total counts); (**III**) DO with (sample E) and without (sample D) TAMRA-fluorophore and with QDs (with BHQ2Quencher) (total counts); (**IV**) normalized comparison of samples C, E, and F. (**V**) Comparison of all samples measured, including a blank glass slide as reference (total counts). For all samples, the DNA origami concentration was set to 10 nM.

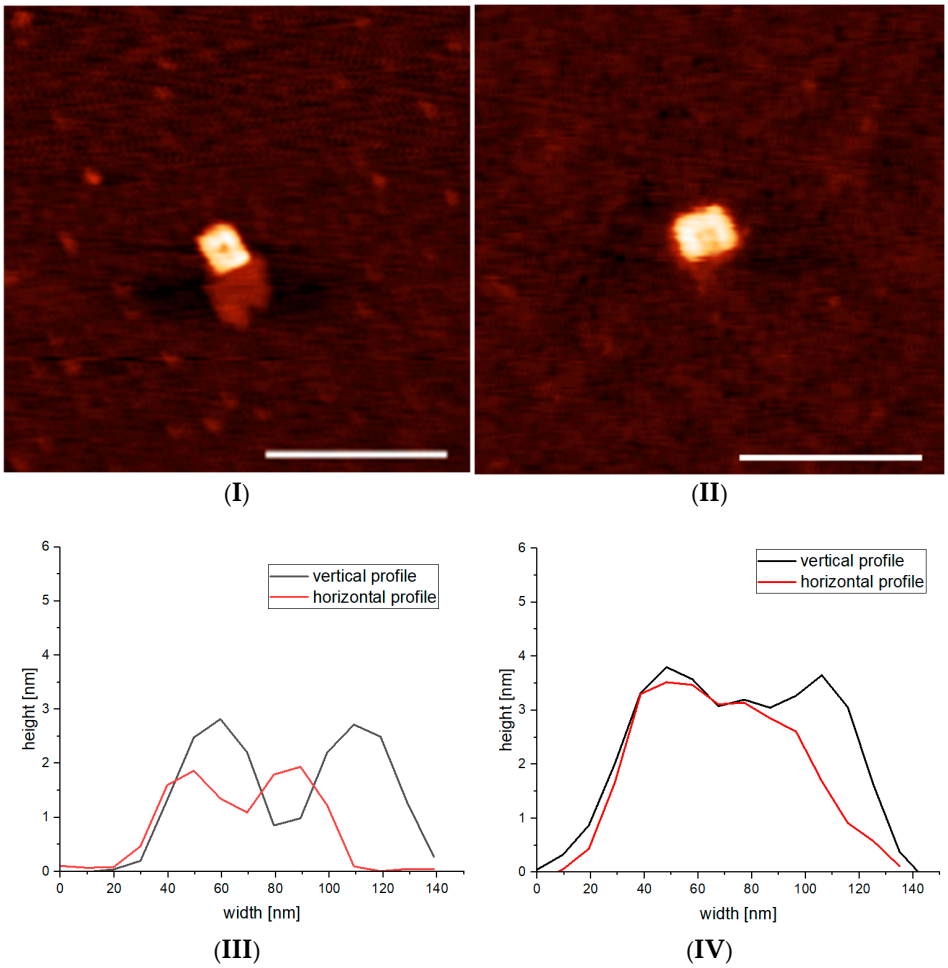


Figure 6. Overview of AFM data gathered from DO without QDs (**I**), as well as purified DO-QD-hybrids (**II**). Scale bar is 500 nm. Bottom row (**III**,**IV**) features the height profile measured for each sample, respectively. All height profiles recorded have been gathered from the center of the structures.

4. Discussion

The confirmation of QD-DNA origami hybridization via AFM proved difficult as the QDs utilized in this experiment had a diameter (d ~ 2–5 nm) similar to the thickness of the frame structure (~2–3 nm).

The hybridization sequences were designed with robust annealing in mind. To this end, minor irregularities such as a single base pair mismatch or incomplete hybridization could potentially go undetected as they would not disrupt the overall annealing, as the complementary segment is 23 bases long. Xu et al. were able to show [22,23] that annealing is significantly more robust for sequences > 15 bases. Furthermore, the base sequences were designed not to show significant sequence similarity (<8 bases) to any staple strand in order to minimize unintended annealing.

While visual confirmation of hybridization was possible for Figure 6II, AFM image data often times is not conclusive enough for confirmation. The verification via photoluminescence as presented in this paper proved to be a more efficient way to confirm successful hybridization as well as purification of hybrid structures from solutions. Through the utilization of FRET fluorophore–quencher pairs, successful hybridization of nanoobjects to DNA origami structures can be confirmed. This proved to be possible even for nanoobjects with dimensions similar to those of DNA origami structures that might not be distinctively detectable by the means of AFM validation. However, it should be considered that the combination of fluorophore and quencher, their respective emission and excitation peaks,

as well as the choice of each for either nanoobject or DNA origami structure may influence the quality of the results [24]. In this experiment, it was chosen to add the quencher to the QD-DNA sequences, as the QDs emission peak was near the peak of the fluorophore and thus might have made distinction of labeled and unlabeled QDs difficult. Ideally, for the hybridization with a nanoobject, which exhibits photoluminescence of itself, the FRET pair should be chosen regarding the best peak separation of the QD emission and the fluorophore. Still, as was proven in this paper, even for QDs and fluorophores with emission peaks relatively close to each other, this method can be utilized to successfully validate DNA origami nanoobject hybridization. While the fluorophores and QDs emission result in the formation of a single emission peak, it is still distinctively different from either component isolated emission peaks and can be differentiated using spectral analysis.

While the presented FRET-based hybridization validation methodology offers a robust and targeted approach for confirming the assembly of DNA origami–quantum dot hybrid structures, several limitations and considerations must be acknowledged.

The current resolution for validating origami structure correctness is primarily determined by a combination of photoluminescence spectroscopy and atomic force microscopy (AFM). While AFM provides nanometer-scale topographical information, its ability to distinguish between the QD and the DNA origami is limited when their dimensions are similar, as is the case in this work (QD diameter $\approx$ 2–5 nm, origami thickness $\approx$ 2–3 nm). However, this can be extended by using high-resolution measuring tips (SuperSharp Tips, tip radius ~2 nm). Photoluminescence measurements, on the other hand, offer molecular-level confirmation of functional hybridization but do not directly resolve structural details beyond the presence or absence of the designed FRET interaction. However, it should be noted that the glass substrate used for PL measurements showed some photo luminescence of its own.

Due to the experimental setup of the PL measurements, absolute light intensity could not directly be compared, resulting in differences between similar samples.

Therefore, below a certain sample concentration, unwanted photons emitted from the glass substrate can "overgrow" the photons emitted from the samples. Thus, the ultimate resolution for structural validation is constrained by both the physical limits of AFM and the specificity of the optical readout.

Compared to established methods such as DNA-PAINT and STORM, the herein presented method is more focused and specialized towards nanostructure hybridization, as only the relevant sequences (hybridization sequences, see Section C) are labeled with the FRET-pair molecules. As this research is part of the Horizon2020-funded "GREENER" Project, the subsequent aim of this research is to build a QD-LED. Therefore, it was important to utilize an evaluation method, which introduced minimal modifications to the QD as well as the DNA origami, so as not to influence the electrical actuation of the QDs [14].

5. Conclusions

In summary, the approach presented here provides a practical and efficient solution for the validation of DNA origami–quantum dot hybridization, with high specificity and minimal sample requirements. The PL measurements from purified hybrid structures confirmed the successful hybridization of ODs and DOs. However, limitations regarding spectral crosstalk, structural resolution, and the detection of subtle hybridization errors must be considered. Future work may integrate complementary techniques or improved probe design to further enhance the robustness and resolution of origami hybridization validation.

Importantly, beyond validating the assembly, our AFM results demonstrate that DNA origami can serve as a highly efficient and programmable template for positioning single quantum dots with nanometer precision. This controlled spatial organization provides

a robust foundation for engineering nanostructures with tailored photonic properties. The ability to reliably template individual QDs opens new opportunities for quantum-optical device architectures, photonic coupling studies, nanoscale light–matter interaction experiments, and the bottom-up fabrication of functional optoelectronic components. As such, the methodology presented here offers not only a means of verification but also a solid route toward advanced applications where defined placement of quantum emitters is essential.

For future research, additional Dynamic Light Scattering (DLS) data will be taken into account as a further method of identifying successful hybridizations.

Author Contributions: Conceptualization, C.R.M., M.J. and J.H.; methodology, A.D.M., G.K., J.H., M.J. and M.M.; software, M.J.; validation, J.H., D.R. and A.L.C.; formal analysis, M.J. and M.M.; investigation, A.D.M., M.J. and M.M.; resources, A.L.C. and D.R.; data curation, A.D.M., M.J. and M.M.; writing—original draft preparation, A.D.M., G.K., J.H. and M.J.; writing—review and editing, A.L.C., A.D.M., C.R.M., G.K., J.H., M.J. and M.M.; visualization, A.D.M., G.K. and M.J.; supervision, A.M., C.R.M. and J.H.; project administration, A.L.C. and D.R.; funding acquisition, J.H., A.M., A.L.C. and D.R. All authors have read and agreed to the published version of the manuscript.

Funding: Funded by the European Union under grant agreement No. 964248 and 101191980, respectively. The views and opinions expressed are those of the author(s) only and do not necessarily reflect those of the European Union or the European Health and Digital Executive Agency (HADEA). Neither the European Union nor the granting authority can be held responsible for them.

Data Availability Statement: The original contributions presented in this study are included in the article. Further inquiries can be directed to the corresponding author.

Acknowledgments: We thank the technical and administrative staff of the Research Center for Materials, Architectures, and Integration of Nanomembranes (MAIN) for providing access to the laboratory infrastructure and for creating a productive working environment.

Conflicts of Interest: The authors declare no conflict of interest.

References

1. Seeman, N.C. Nucleic acid junctions and lattices. *J. Theor. Biol.* **1982**, *99*, 237–247. [CrossRef]
2. Rothemund, P.W.K. Folding DNA to create nanoscale shapes and patterns. *Nature* **2006**, *440*, 297–302. [CrossRef] [PubMed]
3. Castro, C.E.; Kilchherr, F.; Kim, D.-N.; Shiao, E.L.; Wauer, T.; Wortmann, P.; Bathe, M.; Dietz, H. A primer to scaffolded DNA origami. *Nat. Methods* **2011**, *8*, 221–229. [CrossRef]
4. Zhan, P.; Peil, A.; Jiang, Q.; Wang, D.; Mousavi, S.; Xiong, Q.; Shen, Q.; Shang, Y.; Ding, B.; Lin, C.; et al. Recent Advances in DNA Origami-Engineered Nanomaterials and Applications. *Chem. Rev.* **2023**, *123*, 3976–4050. [CrossRef]
5. Houtepen, A.J.; Sargent, E.H.; Infante, I.; Owen, J.S.; Green, P.B.; Schaller, R.D.; Hens, Z. Colloidal quantum dots for optoelectronics. *Nat. Rev. Methods Primers* **2025**, *5*, 42. [CrossRef]
6. Moebius, M.; Martin, J.; Hartwig, M.; Baumann, R.R.; Otto, T.; Gessner, T. Using quantum dot photoluminescence for load detection. *AIP Adv.* **2016**, *6*, 085309. [CrossRef]
7. Chuang, C.-H.M.; Brown, P.R.; Bulović, V.; Bawendi, M.G. Bawendi. Improved performance and stability in quantum dot solar cells through band alignment engineering. *Nat. Mater.* **2014**, *13*, 796–801. [CrossRef] [PubMed]
8. García de Arquer, F.P.; Talapin, D.V.; Klimov, V.I.; Arakawa, Y.; Bayer, M.; Sargent, E.H. Semiconductor quantum dots: Technological progress and future challenges. *Science* **2011**, *373*, eaaz8541. [CrossRef] [PubMed]
9. Du, K.; Park, M.; Ding, J.; Hu, H.; Zhang, Z. Sub-10 nm patterning with DNA nanostructures: A short perspective. *Nanotechnology* **2017**, *28*, 442501. [CrossRef]
10. Shaw, A.; Benson, E.; Högberg, B. Purification of Functionalized DNA Origami Nanostructures. *ACS Nano* **2015**, *9*, 4968–4975. [CrossRef]
11. Gómez-García, P.A.; Garbacik, E.T.; Otterstrom, J.J.; Garcia-Parajo, M.F. Excita-tion-multiplexed multicolor superresolution imaging with fm-STORM and fm-DNA-PAINT. *Proc. Natl. Acad. Sci. USA* **2018**, *115*, 12991–12996. [CrossRef]
12. Swaraj, S.; Mishra, A. Understanding Photoluminescence Spectroscopy: Principles, Applications, and Insights into Material Properties. In *Smart Materials for Energy Storage and Biomedical Applications*; Engineering Materials; Springer: Cham, Switzerland, 2025; pp. 163–186.

13. Sinha, C.; Arora, K.; Moon, C.S.; Yarlagadda, S.; Woodrooffe, K.; Naren, A.P. Förster Resonance Energy Transfer—An approach to visualize the spatiotemporal regulation of macromolecular complex formation and compartmentalized cell signaling. *Biochim. Biophys. Acta (BBA)—Gen. Subj.* **2014**, *1840*, 3067–3072. [CrossRef] [PubMed]
14. Hann, J.; Moebius, M.; Meinecke, C.; Janssen, M.; Gottwald, M.; Morschhauser, A.; Martin, J.; Murkina, A.D.; Cortajarena, A.L.; Reuter, D. DNA Origami Based Approach for an Electrically Driven Single-Photon Source for Contaminant Detection in Water. In Proceedings of the 2025 Smart Systems Integration Conference and Exhibition (SSI), Prague, Czech Republic, 8–10 April 2025; pp. 1–6. [CrossRef]
15. Douglas, S.M.; Marblestone, A.H.; Teerapittayanon, S.; Vazquez, A.; Church, G.M.; Shih, W.M. Rapid prototyping of 3D DNA-origami shapes with caDNAno. *Nucleic Acids Res.* **2009**, *37*, 5001–5006. [CrossRef]
16. Haggenmueller, S.; Matthies, M.; Sam, M. How We Simulate DNA Origami. *Small Methods* **2025**, *9*, e2401526. [CrossRef]
17. Kim, D.-N.; Kilchherr, F.; Dietz, H.; Bathe, M. Quantitative prediction of 3D solution shape and flexibility of nucleic acid nanostructures. *Nucleic Acids Res.* **2012**, *40*, 2862–2868. [CrossRef]
18. Delices, A.; Moodelly, D.; Hurot, C.; Hou, Y.; Ling, W.L.; Saint-Pierre, C.; Gasparutto, D.; Nagues, G.; Reiss, P.; Kheng, K. Aqueous synthesis of DNA-functionalized near-infrared $AgInS_2$/ZnS core/shell quantum dots. *ACS Appl. Mater. Interfaces* **2020**, *12*, 44026–44403. [CrossRef]
19. Necas, D.; Klapetek, P. Gwyddion: An open-source software for SPM dataanalysis. *Open Phys.* **2012**, *10*, 181–188. [CrossRef]
20. Poppleton, E.; Romero, R.; Mallya, A.; Rovigatti, L.; Šulc, P. OxDNA.org: A public webserver for coarse-grained simulations of DNA and RNA nanostructures. *Nucleic Acids Res.* **2021**, *49*, W491–W498. [CrossRef]
21. Zadegan, R.M.; Lindau, E.G.; Klein, W.P.; Green, C.; Graugnard, E.; Yurke, B.; Kuang, W.; Hughes, W.L. Twisting of DNA Origami from Intercalators. *Sci. Rep.* **2017**, *7*, 7382. [CrossRef]
22. Xu, S.; Zhan, J.; Man, B.; Jiang, S.; Yue, W.; Gao, S.; Guo, C.; Liu, H.; Li, Z.; Wang, J.; et al. Real-time reliable determination of binding kinetics of DNA hybridization using a multi-channel graphene biosensor. *Nat. Commun.* **2017**, *8*, 14902. [CrossRef] [PubMed]
23. Stein, J.A.C.; Ianeselli, A.; Braun, D. Kinetic Microscale Thermophoresis for Simultaneous Measurement of Binding Affinity and Kinetics. *Angew. Chem.* **2021**, *60*, 13988. [CrossRef] [PubMed]
24. Pillai, S.S.; Yukawa, H.; Onoshima, D.; Biju, V.; Baba, Y. Fluorescence Quenching of CdSe/ZnS Quantum Dots by Using Black Hole Quencher Molecules Intermediated with Peptide for Biosensing Application. *Cell Med.* **2017**, *8*, 57–62. [CrossRef] [PubMed]

Disclaimer/Publisher's Note: The statements, opinions and data contained in all publications are solely those of the individual author(s) and contributor(s) and not of MDPI and/or the editor(s). MDPI and/or the editor(s) disclaim responsibility for any injury to people or property resulting from any ideas, methods, instructions or products referred to in the content.